# UC Santa Barbara
## UC Santa Barbara Previously Published Works

**Title**

Characterization of electrostatically coupled microcantilevers

**Permalink**

https://escholarship.org/uc/item/5sb85255

**Journal**

Journal of Microelectromechanical Systems, 14(2)

**ISSN**

1057-7157

**Authors**

Napoli, Mariateresa
Zhang, W H
Turner, K
et al.

**Publication Date**

2005-04-01

Peer reviewed

# Characterization of Electrostatically Coupled Microcantilevers

Mariateresa Napoli, Wenhua Zhang, *Student Member, IEEE, Student Member, ASME*,
Kimberly Turner*, Member, IEEE, Member, ASME*, and Bassam Bamieh*, Senior Member, IEEE*

*Abstract*—The use of tightly packed arrays of probes can achieve the much desirable goal of increasing the throughput of scanning probe devices. However the proximity of the probes induces coupling in their dynamics, which increases the complexity of the overall device. In this paper we analyze and model the behavior of a pair of electrostatically and mechanically coupled microcantilevers. For the common case of periodic driving voltage, we show that the underlying linearized dynamics are governed by a pair of *coupled Mathieu* equations. We provide experimental evidence that confirms the validity of the mathematical model proposed, which is verified by finite element simulations as well. The coefficients of electrostatic and mechanical coupling are estimated respectively by frequency identification methods and noise analysis. Finally, we discuss parametric resonance for coupled oscillators and include a mapping of the first order coupled parametric resonance region.                                                        **[1253]**

*Index Terms*—Electrostatically actuated microcantilevers, multiprobe devices, parametric resonance, system identification.

## I. INTRODUCTION

**O**VER the past years, research in the field of scanning probe technology and electromechanical devices in general, has been characterized by two main trends, namely miniaturization and parallelizing. Indeed, the use of array architectures of micro probes not only significantly increases the throughput of the device, it enhances its functionality as well, allowing for more complex, multipurpose instruments. Examples of such devices can be found in data storage and retrieval applications [1], biosensors [2], and multiprobe scanning devices [3] to cite but a few.

Currently, these multiprobe devices are designed with large spacing between the individual elements [1]–[6]. This essentially decouples the dynamics of the individual probes, that can be considered to behave as isolated units. The drawback of this configuration is, of course, a decrease in the potential throughput of the system.

The device that we consider in this paper consists of a pair of closely spaced microcantilevers. The extension to the case of an array of tightly packed cantilevers is not conceptually difficult and is obtained as a generalization of the analysis we present here. Cantilever geometries are particularly interesting, due to

their wide range of applications, including small force detection [7], [8], AFM, mechanical filters for telecommunication [9]–[12], and chemical sensor arrays [13]. In our design each microcantilever constitutes the movable plate of a capacitor and its displacement is controlled by the voltage applied across the plates. We have preferred capacitive actuation over other integrated schemes (e.g., piezoelectric [5], [6], [14], piezoresistive [15], [16], thermal [17]) because it offers both electrostatic actuation as well as integrated detection, without the need for an additional position sensing device. As a matter of fact, we are currently studying the implementation of a detection scheme for displacement based on the measurement of the current through the cantilevers [18].

In this paper we present a mathematical model that explicitly incorporates the dynamical coupling between the microcantilevers. Using simple parallel plate theory and for the common case of sinusoidal forcing, we have demonstrated [19] that the dynamics of each isolated cantilever are governed by a Mathieu equation. Here we show that the close spacing and the fact that the cantilevers are connected to a common base introduces a coupling in their dynamics, which is both electrostatic and mechanical. In particular, we show that the system is governed by a pair of *coupled Mathieu* equations. We produce experimental evidence that validates the mathematical model proposed, including a mapping of the first instability region of the Mathieu equation. The natural frequency of each isolated beam and the electrical and mechanical coupling coefficients are determined from the identification of the experimental data. These results are also validated by finite element simulation methods.

The paper is organized as follows. In Section II, we develop the mathematical model of the electrostatically actuated cantilever pair. In Section III, we present the experimental results that validate the model. In the linear regime of operation, we identify from experimental data the coefficients of mechanical and electrostatic coupling. We prove that parametric resonance can be induced in coupled oscillators and include the mapping of the first instability region of the coupled Mathieu equation. In Section IV, finally we present our conclusions.

## II. MODEL DESCRIPTION

Fig. 1 shows the geometry of our device. It consists of two microbeams connected to the same base, each forming a microcapacitor, with the second plates (rigid) placed underneath the (movable) cantilevers visible in the picture. The vertical displacement of each cantilever can be independently controlled by applying a voltage across the plates. Though each cantilever is
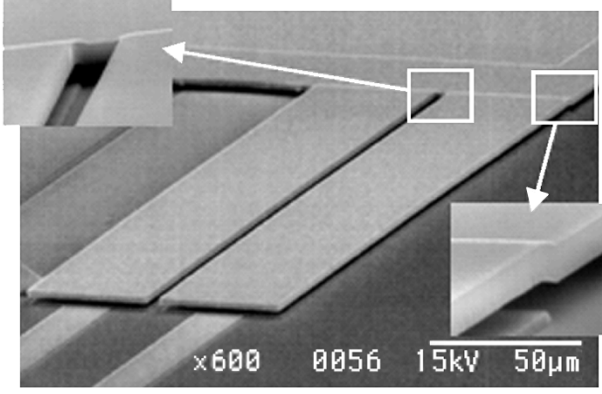
Fig. 1. SEM micrograph of the device. The insets show details of the mechanical connection to the base and between the cantilevers.
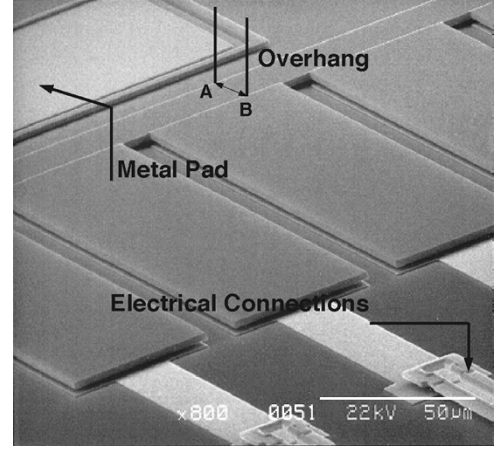


Fig. 2. Micrograph showing the overhang between anchor and cantilevers base, responsible for the mechanical coupling.



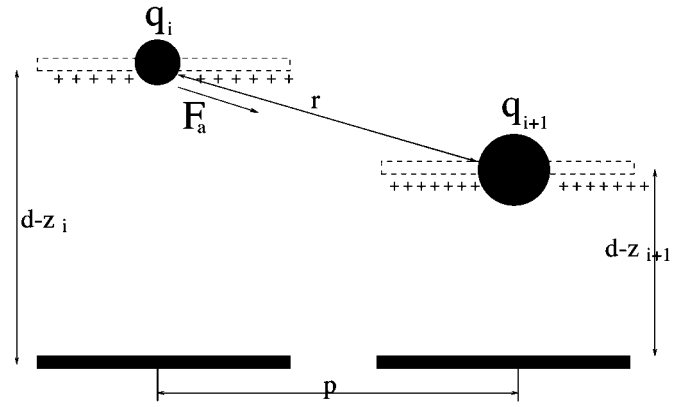Fig. 3. Schematic of the electrostatic coupling model.

independently actuated, its dynamics are influenced by the presence of the other cantilever. More precisely, the coupling is both mechanical, because the microbeams are connected to the same base, and electrostatic, due to the fringing fields generated by the capacitor nearby.

The force acting on each microbeam consists of several components, and the overall linearized equation of motion for the vertical displacement $z_i$, $i = 1, 2$, of each cantilever can be written as

$$\ddot{z}_i + \nu_i \dot{z}_i + \omega_{ri}^2 z_i = F_{e,i} + F_{mc,i} + F_{ec,i}^\perp \qquad (1)$$

where $\nu_i$ and $\omega_{ri}$ are respectively the normalized damping coefficient and the natural resonant frequency of the $i$th cantilever. Here, $F_{e,i}$ expresses the electrostatic force between the capacitor plates of the $i$-th cantilever, while $F_{mc,i}$ and $F_{ec,i}$ are respectively the mechanical and electrostatic coupling forces. By using simple parallel plate theory, the linearized expression of $F_{e,i}$ can be shown to be

$$F_{e,i} = \frac{\epsilon_o A}{2md^2} \left(1 + 2\frac{z_i}{d}\right) V_i^2$$

where $\epsilon_o = 8.85 \, 10^{-12}$ As/Vm is the permittivity in vacuum, $d$ is the gap between the electrodes, $A$ is the area of the capacitor plates, $m$ their mass, and $V_i$ is the voltage applied.

The mechanical coupling force $F_{mc,i}$, which will turn out to be relatively large, originates from the fact that the cantilevers are connected to the base through an overhang as shown in Fig. 2.

For $F_{mc,i}$ we have adopted a lumped-parameters description, and modeled the mechanical coupling force as a spring like force, proportional to the difference in the vertical displacement of the cantilevers

$$F_{mc,i} = \Gamma(z_i - z_j). \qquad (2)$$

The value of $\Gamma$ is a function of both the lateral distance between the probes and the thickness of the overhang. Intuitively, one expects this value to be higher as the lateral distance decreases and the thickness increases. However, the derivation of the exact dependence of $\Gamma$ from these parameters requires to solve the complex PDEs derived from a continuum mechanics description of the problem.

As far as the electrostatic coupling is concerned, we consider that the voltage applied to each capacitor results in a charge induced on each cantilever, that can be expressed as [20]

$$q_i = c_{i,1} V_1 + c_{i,2} V_2 \quad i = 1, 2.$$

The interaction between these induced charges is described via a point charge model. The idea is shown schematically in Fig. 3. Each cantilever is represented as a charged particle $q_i$ and the mutual interaction is described by Coulomb's law

$$F_{ec,i} = \frac{1}{4\pi\epsilon_o} \frac{q_i q_j}{r^2}.$$

We assume that the lateral stiffness of the cantilevers is large enough to prevent any lateral motion, so that the only component of the force that really affects their behavior is the vertical, whose first order approximation is

$$F_{ec,i}^\perp = \left[K_{i,i} V_i^2 + K_{i,j} V_i V_j + K_{j,j} V_j^2\right](z_i - z_j)$$

where the coefficients $K_{m,n}$ have been scaled by the mass, to be consistent with (1).

For the special case of $V_i = V_{oi} \cos \omega t$, and after few algebraic steps, the equation of motion for the pair can be written, in compact vector form as

$$\begin{bmatrix} \ddot{z}_1 \\ \ddot{z}_2 \end{bmatrix} + \begin{bmatrix} \nu_1 & 0 \\ 0 & \nu_2 \end{bmatrix} \begin{bmatrix} \dot{z}_1 \\ \dot{z}_2 \end{bmatrix} + \left\{ \begin{bmatrix} \omega_1^2 & \gamma_1 \\ \gamma_1 & \omega_2^2 \end{bmatrix} + \begin{bmatrix} \epsilon_1 & \gamma_2 \\ \gamma_2 & \epsilon_2 \end{bmatrix} cos(2\omega t) \right\}$$
$$\times \begin{bmatrix} z_1 \\ z_2 \end{bmatrix} = \begin{bmatrix} b_1 & 0 \\ 0 & b_1 \end{bmatrix} \begin{bmatrix} V_1^2 \\ V_2^2 \end{bmatrix}$$

where $\omega_i^2 = \omega_{ri}^2 - \Gamma - (K_e V_{oi}^2 + K_T)$, $\epsilon_i = -(K_e V_{oi}^2 + K_T)$, $\gamma_1 = \Gamma + K_T$, $\gamma_2 = K_T$, $K_T = (K_{11} V_{o1}^2 + K_{12} V_{o1} V_{o2} + K_{22} V_{o2}^2)/2$, $b_1 = K_e d/2$ and $K_e = \epsilon_o A/(md^3)$; or equivalently, introducing the vector $Z = [z_1 \ z_2]^T$, $U = [V_1^2 \ V_2^2]^T$ and defining the appropriate matrices

$$\ddot{Z} + \nu \dot{Z} + [\Delta + \epsilon E cos(2\omega t)] Z = kU, \quad Z \in \mathbb{R}^{2 \times 1} \quad (3)$$

where $\epsilon$ represents a small perturbation parameter. The results presented in the next Section will justify this notation.

Equation (3) represents a system of periodic differential equations, which we refer to as *vector Mathieu equation*, since its algebraic structure is reminiscent of the famous Mathieu equation. In the absence of coupling, they reduce to a pair of independent scalar Mathieu equations, which indeed describe the dynamics of an isolated beam [19]. In the next section, we provide experimental data to validate the model proposed and demonstrate how the coupling, often considered a drawback, can instead be advantageously exploited from an engineering point of view.

### III. EXPERIMENTAL VALIDATION OF THE MODEL

The device we have used in our experimental setup consisted of two $200 \ \mu m \times 50 \ \mu m \times 2 \ \mu m$ highly doped polysilicon cantilevers, fabricated using the MUMPS/CRONOS process [21], with a gap between the electrodes of about $2 \ \mu m$ and separated by a distance of $5 \ \mu m$ (see Fig. 1). The mechanical response of the cantilevers was tested in vacuum ($p = 8$ mtorr), using laser vibrometry [22] to measure displacement and velocity near the free end of each cantilever, when electrostatically driven with different ac voltage signals.

More precisely, the excitation voltage for driving the devices being tested was generated by a power source (Hewlett Packard, HP3245A), while the oscillation velocity and position were measured at the free end of the cantilever using a laser vibrometer (Polytec, OFV 3001, OFV 511). The laser beam is focused onto the device using an optical microscope, which can be positioned over the sample via a computer controlled, mechanical x-y positioning mechanism. The measurement is based on interferometry, in which the idea is to split the laser beam into two (coherent) beams: one that impinges on the device tested, the other on a reference target. The relation between the difference in phase and the difference in path length traversed by the two beams is then translated into displacement of the beam. Due to the relatively high working frequency and the small displacement of the cantilevers ($f \approx 50$ kHz and $x = O(\text{nm})$), we worked with velocity measurements, which for high frequencies are more reliable and accurate than position measurements [23].

The results of these measurements were recorded and analyzed with a signal analyzer (Hewlett Packard, HP89410A) and
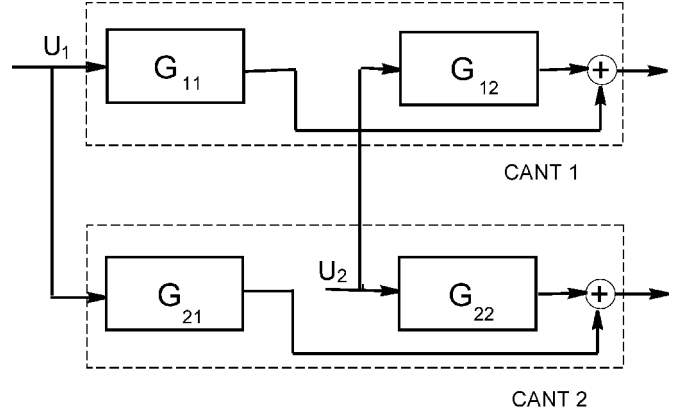


Fig. 4. Schematic of the system transfer functions.

oscilloscope (Tektronics, TDS 420A). The instruments were interfaced to a PC, where data could be stored for further analysis.

### A. Linear Regime of Operation

The first set of experiments was performed to characterize the system in its linear regime of operation, that is for small input signals ($V_{oi} \leq 1$ V). When the amplitude of the voltage applied $V_{oi}$ in (3) is small, the time-varying coefficients can be neglected and the device is described by a system of second order ordinary differential equations

$$\ddot{Z} + \nu \dot{Z} + \Delta Z = kU. \quad (4)$$

Because of the coupling, the vibration of each cantilever depends both on its input and on the voltage applied to the other cantilever. Therefore each cantilever is characterized by two transfer functions, that describe how each input affects its dynamical behavior. Let Gij denote the transfer function from the voltage input applied to the $j$th cantilever to the velocity output measured on the $i$th cantilever, when the other voltage input is set to zero (see Fig. 4 for a schematic representation). The analytical expression of these transfer functions can be found to be

$$G_{ii} = \frac{b_1 s \left( s^2 + \nu_i s + \omega_{z_i}^2 \right)}{\left( s^2 + a_{1i} s + \omega_{pk1}^2 \right) \left( s^2 + a_{2i} s + \omega_{pk2}^2 \right)}$$
$$G_{ij} = \frac{c_i s}{\left( s^2 + a_{1i} s + \omega_{pk1}^2 \right) \left( s^2 + a_{2i} s + \omega_{pk2}^2 \right)} \quad (5)$$

where $a_{1i} = \nu_i$, $\omega_{pk1}^2 = \omega_{ri}^2 - \Gamma - (K_e - K_{ii})V_{oi}^2$, $a_{2i} = \nu_j$, $\omega_{pk2}^2 = \omega_{rj}^2 - \Gamma + K_{ii}V_{oi}^2) - (\Gamma - K_{ii}V_{oi}^2)^2$, $c_i = b_1(\Gamma - K_{ii}V_{oi}^2$ and $\omega_{z_i}^2) = \omega_{ri}^2 - \Gamma + K_{ii}V_{oi}^2$. Fig. 5 represents the experimental and fitted data of these frequency responses. Notice the presence of two peaks in the frequency response of each single cantilever, a consequence of coupling, predicted by (5) as well. These frequencies correspond to the so-called normal modes of the system and their values coincide approximately to $\omega_{pk1}$ and $\omega_{pk2}$, respectively. It can be proved that the oscillation of the microbeams is in phase for $\omega = \omega_{pk1}$ and in antiphase for $\omega = \omega_{pk2}$ [24].

By fitting our model to the experimental data, as shown in Fig. 5, we get that the natural resonant frequencies of the isolated beams are, respectively, $\omega_{r1} = 48\,870$ Hz and $\omega_{r2} =$
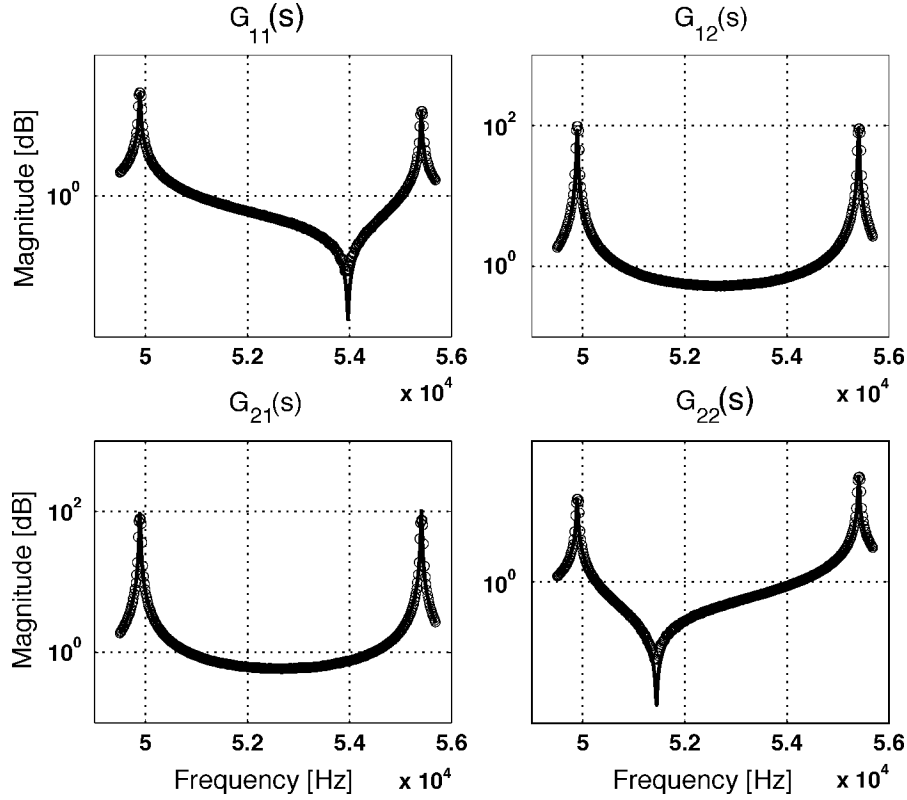
Fig. 5. Magnitude of the frequency responses of the coupled cantilevers with different input/output combinations. The circles represent experimental data; the solid line the fitted data.

51 520 Hz, while the quality factors turn out to be $Q_1 = Q_2 \approx 3000$. The difference in the values of $\omega_{r1}$ and $\omega_{r2}$, in spite of the fact that the beams have the same geometry and material, is to be attributed to the asymmetry of the anchor in the point where it connects to the beams, visible in Fig. 1 and also in the Ansys model of Fig. 8.

*1) Identification of Mechanical and Electrostatic Coupling Coefficients:* The coefficient of mechanical coupling $\Gamma$ has been estimated using the power spectral density (PSD) of the vibrations induced by thermal noise. By setting to zero both inputs, the electrostatic coupling is eliminated and the effect of $\Gamma$ can be singled out. More precisely, the location of the peaks in the frequency responses is in this case solely determined by $\Gamma$. Fig. 6(c) and (d) shows the experimental characterization of noise, that as expected has a gaussian distribution. From stochastic filtering theory it is known that the PSD $S_y$ of the output of a linear system $G$ excited by random noise $e$ is given by

$$S_y(\omega) = G(\omega)G(\omega)^* S_e(\omega) = |G(\omega)|^2 S_e(\omega) \qquad (6)$$

where $S_e$ is the PSD of the input noise. In our case, since the system has two inputs, and the noise on each of them is mutually independent, (6) becomes

$$S_{y_i}(\omega) = |G_{ii}(\omega)|^2 S_{e_i}(\omega) + |G_{ij}(\omega)|^2 S_{e_j}(\omega),$$
$$= \left( |G_{ii}(\omega)|^2 + |G_{ij}(\omega)|^2 \right) S_e(\omega) \qquad (7)$$

where the last equality follows from the fact that $e_1$ and $e_2$ have the same stochastic description. Since the PSD $S_e$ of thermal

noise is constant, (7) offers a way to extrapolate the value of $\Gamma$ from the value of the normal modes. Parts a), b) of Fig. 6 show the comparison between measured and fitted data after (7). Note that the region between the two peaks is below the noise level of our instrumentation, hence a good fit cannot be obtained.

By examining the numerator of $G_{11}$ and $G_{22}$ in (5), one can notice the presence of a resonant zero, visible also in Fig. 5 as a dip in the magnitude plot of these functions. This zero frequency is called antiresonance [24], and its value is approximately equal to $\omega_{zi}^2 = \omega_{ri}^2 - \Gamma + K_{ii}V_{oi}^2$. This expression highlights that its existence is due to the mechanical and electrostatic coupling, and its location changes with the amplitude of the driving voltage. This property gave us a way to estimate the values of the electrostatic coefficients $K_{11}$ and $K_{22}$, as shown in Fig. 7(a) and (b). As a matter of fact, the shift in the zero location depends linearly on the voltage applied, and the coefficient of proportionality is given by $K_{11}$ for $G_{11}$ and $K_{22}$ for $G_{22}$. In a similar fashion, the coefficient $K_e$ was estimated from the shift in the poles with the applied ac voltage. Finally, the coefficient $K_{12}$ was estimated by applying the same voltage to both inputs. In this case the system is specified by only two transfer functions, whose analytical expression can be easily derived from (4). In particular, the numerator of the transfer function of cantilever 1 turns out to be

$$n_1(s) = b_1 s \left( s^2 + \nu_2 s + \omega_{r2}^2 - 2\Gamma - K_e V_o^2 + 2K_T \right)$$
$$= b_1 s \left( s^2 + \nu_2 s + \tilde{\omega}_{z1}^2 \right)$$

therefore also in this case the location of the antiresonance is related to the changes in amplitude of the ac voltage applied $V_o$.
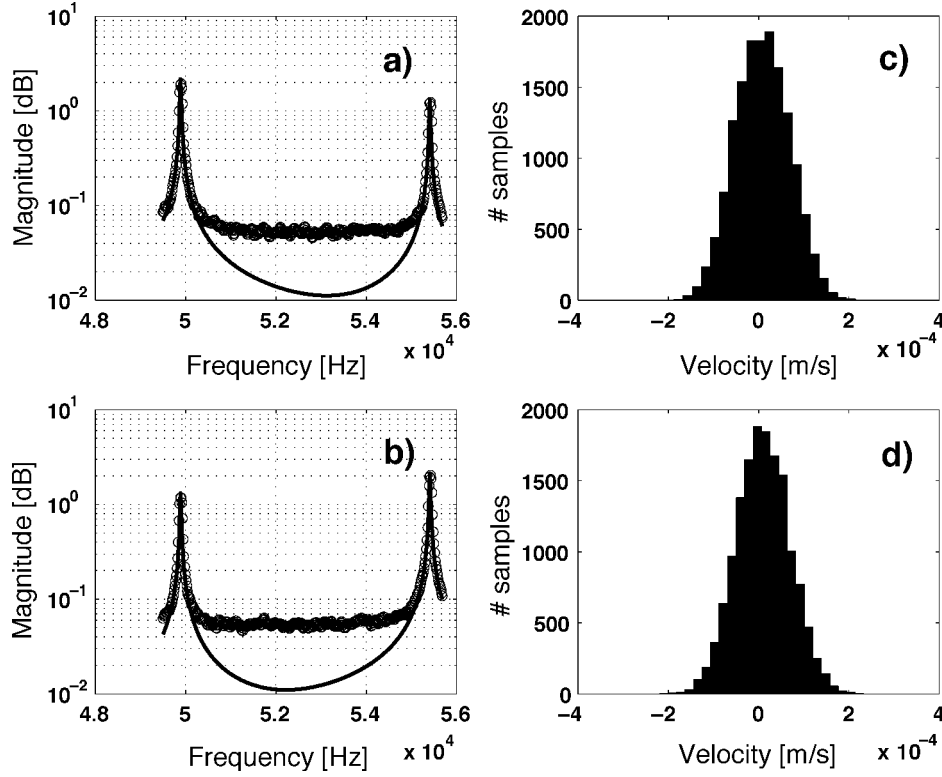
Fig. 6.  (a) and (b) Fit from PSD of thermal noise to determine $\Gamma$. Circles denote experimental data, the solid line is the fit. (c) and (d) Experimental characterization of noise distribution ($10^4$ samples of the noise signal at the vibrometer output).

It is worth noting that the equivalent stiffnesses corresponding to these electrostatic coupling parameters are quite large, indicating significant coupling in this system, but two orders of magnitude smaller than the mechanical stiffness of the uncoupled cantilever, justifying the notation of (8), where they are represented as a perturbation to a time invariant equation.

*2) Finite Element Simulations:* We have performed some simulations using finite element methods to verify the experimental findings. The pair of cantilevers has been modeled according to the actual physical configuration, as shown in Fig. 1. In particular, both the anchor and the overhang which connects the two beams have been explicitly incorporated in the model. The geometry generated in Ansys is shown in Fig. 8(a). The values of the first two modes, found by modal analysis using the element *Solid*92, match well the values of the two peaks in the frequency response found experimentally. Fig. 8(b) and (c) shows the Ansys model corresponding to the isolated cantilevers. These models have been used to determine the resonant frequency of the uncoupled cantilevers. Table I presents the value of some significant parameters obtained by identification and compares it with the value obtained by finite elements simulation. The agreement is quite satisfactory.

As the amplitude of the driving signal increases, so do the values of $\epsilon_i$ and $\gamma_2$ and this linear time-invariant approximation of the system is no longer appropriate. In order to predict and explain the rich dynamics that the system shows, we have to return to the original (3).

### B. Parametric Resonance

Parametric resonance is a form of mechanical amplification that can be induced in systems having periodically varying parameters. In this mode of operation, large responses can be generated even when the excitation frequency is far away from the system's natural frequency. The interest from an engineering point of view for this phenomenon comes from the fact that it can greatly enhance the sensitivity of microdevices, which as their size reduces, find themselves operating closer to noise level [25].

In [19] we showed that a single electrostatically actuated microcantilever can exhibit parametric resonance, whose existence in MEMS devices was first demonstrated in [26]. In this section we demonstrate that this phenomenon persists also in the case of coupled cantilevers [27], [28].

Ignoring damping and external excitations, (3) can be written as

$$\ddot{Z} + [\Delta + \epsilon E cos(2\omega t)] Z = 0 \quad Z \in \mathbb{R}^{2 \times 1} \quad (8)$$

which can be considered the vector extension of a standard Mathieu equation. Parametric amplification depends on the stability properties of (8), and more precisely on the stability of its periodic solutions [29]. It can be shown that the stability of these trajectories is equivalent to the stability of the equilibrium points of the discrete time-invariant system having as its state matrix the state transition matrix of (8) computed at the period,
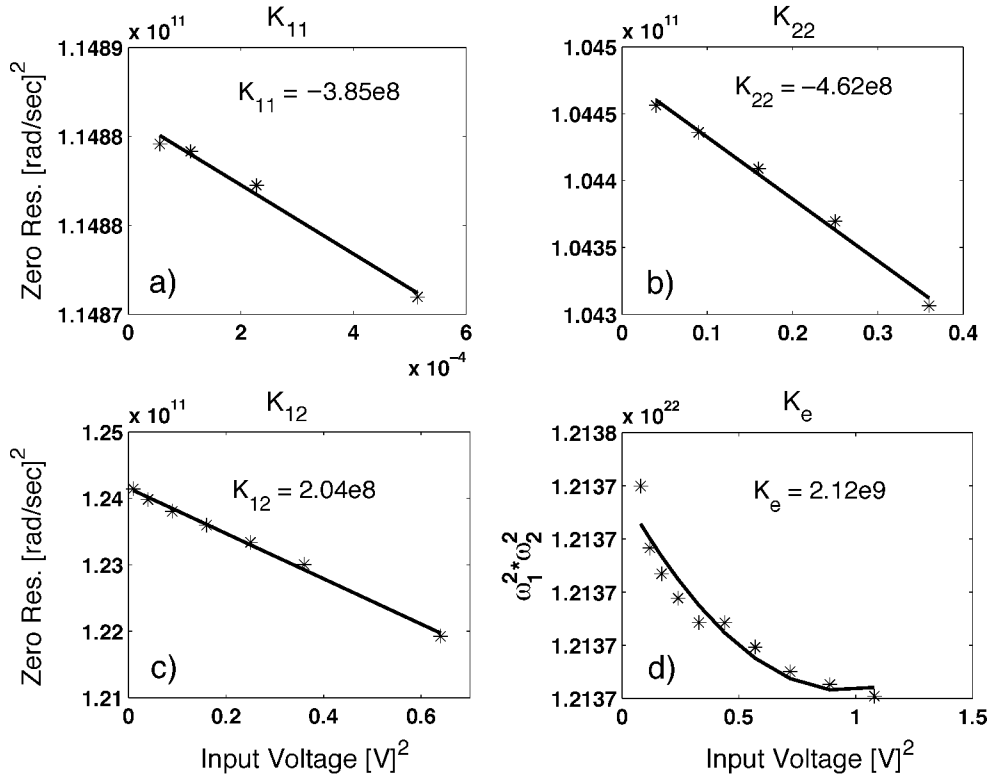
Fig. 7.   Experimental estimation of the electrostatic coefficients. $K_{ij}$ are the coefficients of the electrostatic coupling force, $F_{ec,i}$; $K_e$ is the coefficient of the attractive force, $F_{e,i}$, between the cantilever and its ground plate.
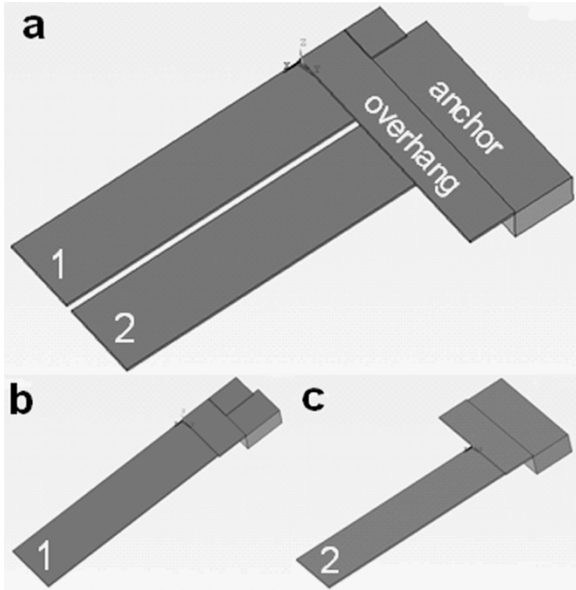


Fig. 8.   Ansys model of the cantilever pair (a) and of the single cantilevers (b) and (c).
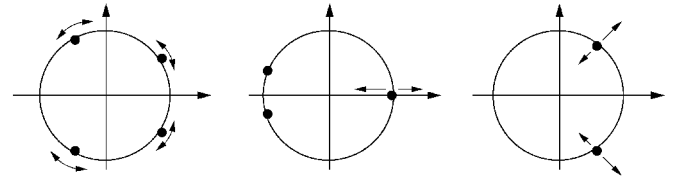


Fig. 9.   Schematic representation of the conditions corresponding to a possible loss in stability for two coupled Mathieu equations.

$\Phi(T)$. In the following, we show that for $\epsilon = 0$ in (8) the origin is a strongly stable (for a Definition see [29, p. 117]) equilibrium point of $\Phi(T)$. Then, by definition, the 'perturbed' solution, obtained for small values of $\epsilon$, will be stable as well.

For $\epsilon = 0$, (8) is time-invariant and describes a two-dimensional harmonic oscillator

$$\ddot{Z} + \Delta Z = 0. \tag{9}$$

The eigenvalues $\mu_j$ of the $\Phi(T)$ corresponding to this equation are given by

$$\mu_j = e^{\lambda_j T}, \quad j = 1, \dots, 4 \tag{10}$$

where the $\lambda_j$'s are the eigenvalues of a state space representation of (9) and are purely imaginary pairs, since there is no damping. As a consequence, the $\mu_j$'s are on the unit circle. By virtue of Liouville's theorem, the product of the $\mu_j$'s, for any value of $\epsilon$, is always equal to 1. Together, these two facts imply that the origin is strongly stable. As a matter of fact, these conditions constrain the eigenvalues of the perturbed state transition matrix to move in complex conjugate pairs along the unit circle, and therefore

TABLE  I

COMPARISON BETWEEN THE VALUE OBTAINED BY TESTING AND FINITE ELEMENT SIMULATIONS OF SOME RELEVANT PARAMETERS OF THE MODEL

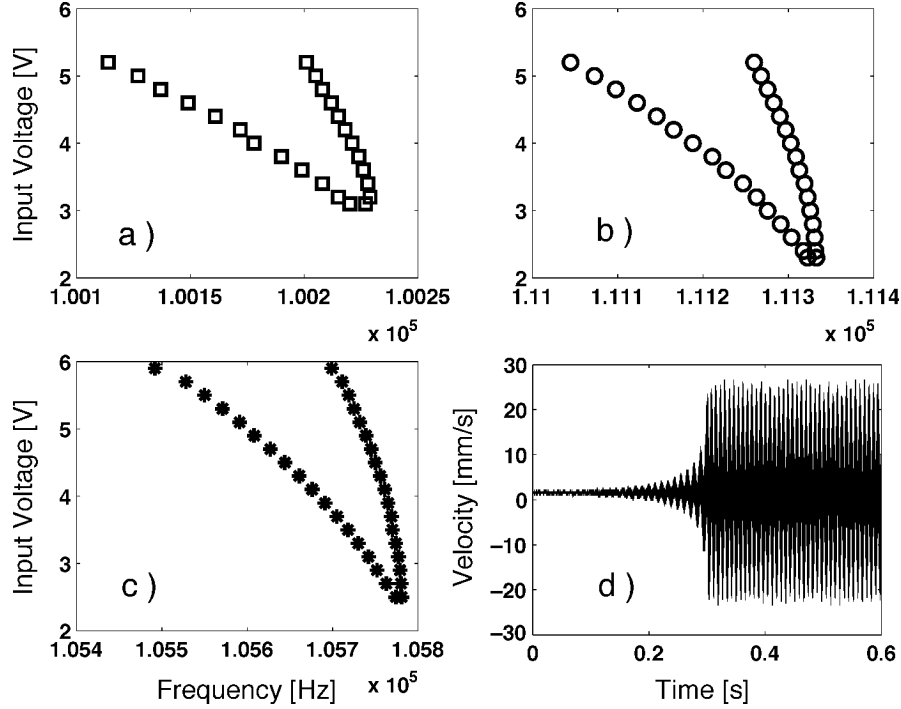|         | $\omega_{pk1}$ | $\omega_{pk2}$ | $\omega_{r1}$ | $\omega_{r2}$ | $\Gamma$ |
|---------|-------|-------|-------|-------|----------|
| FEM     | 50045 | 55868 | 48830 | 51681 | $1.10e^{10}$ |
| Testing | 48896 | 55417 | 48870 | 51520 | $1.02e^{10}$ |
| Error   | 2.3%  | 0.8%  | 0.1%  | 0.3%  | 7.8%     |

Fig. 10.   First region of coupled parametric amplification, with the electric signal applied to one cantilever only. The three tongues correspond respectively to (a) $\omega = 2w_{pk1}$; (b) $\omega = 2w_{pk2}$; (c) $\omega = w_{pk1} + w_{pk2}$. Picture (d) shows the exponential growth of the output inside the region of parametric amplification.

describe stable dynamics. The only cases when the perturbed system can have unstable eigenvalues, is when at least one pair of $\mu$'s overlaps and is equal to $\pm 1$, or when the two pairs of $\mu$'s overlap, as represented schematically in Fig. 9. In fact, in these cases the $\mu$'s can leave the unit circle, still satisfying the condition on their product.

This loss of stability corresponds to the cases $|\lambda_j|T = \pi n$, and $(|\lambda_i| \pm |\lambda_j|)T = 2\pi n$, $n \in \mathbb{N}$. It is not difficult to prove that

$$|\lambda_j| = \sqrt{\eta_i} \quad i = 1, 2$$

where the $\eta$'s are the eigenvalues of $\Delta$, and correspond roughly to the resonant frequencies $\omega_{pk1}$ and $\omega_{pk2}$, defined in Section III-A.

Hence, in terms of frequency of excitation, parametric resonance can occur when

$$\omega = \frac{\omega_{pki}}{n}, \quad \omega = \omega_{pk1} \pm \frac{\omega_{pk2}}{2n} \qquad n \in \mathbb{N}. i = 1, 2. \quad (11)$$

It follows that, similarly to the case of a scalar Mathieu equation, the $\epsilon$–$\omega$ parameter space can be divided into tongue-shaped parametric/nonparametric regions. The $\omega$ values in (11) correspond to the tips of these regions. More precisely, according to (11) each region of parametric amplification (i.e., each $n$) for two coupled Mathieu equations is composed of four subtongues. In fact, in [30], [31] the authors proved that $\omega = \omega_{pk1} - \omega_{pk2}/2n$ is never a critical value, i.e. cannot excite a parametric behavior.

Note that the presence of a damping term, whose existence we have neglected so far, has the effect of shifting the tongues upwards, so that there is a critical voltage amplitude above which parametric resonance can be induced [32], but does not affect the stability analysis.

Fig. 10 shows the experimental mapping of the first region $(n = 1)$ for our pair of cantilevers, where in terms of physical parameters, $\epsilon$ corresponds to the input voltage amplitude $V_o$. During these experiments one of the inputs was set to zero, while the other was set to $V_i = (V_o/2)\sqrt{1 + \cos \omega_o t}$. Which input is selected is in fact inconsequential, given the symmetry of the device, and the results can be reproduced using either one of them. Note that when the input is a square-rooted sinusoid, (11) needs to be modified, to give $\omega = 2\omega_{pk,i}/n$ and $\omega = (\omega_{pk,1} \pm \omega_{pk,2})/n$. Fig. 10(a) and (b) shows the cases corresponding to the driving frequency being varied around a) $2\omega_{pk1}$, (b) $2\omega_{pk2}$, and (c) $\omega = \omega_{pk1} + \omega_{pk2}$.

During the parametric amplification regime the beams exhibit an oscillation that is bounded by the system nonlinearities [32]. In fact, for large oscillation amplitudes, both the linear spring model and the electrostatic force previously introduced need to be corrected by adding cubic terms [33], [34]. Hence, (3) becomes

$$\ddot{Z} + \nu \dot{Z} + [\Delta + \epsilon E cos(2\omega t)] Z + A_3 Z^3 = kU$$

where the matrix $A_3$, diagonal, describes the effective cubic stiffness of each beam, which includes both electrostatic and structural contributions. What we observe when driving the cantilever in parametric resonance regime is: in case a) and b) a subharmonic 2:1 oscillation at half the frequency of excitation; in case c) an oscillation having both frequency components. Note also that during the transition from nonparametric to parametric region, the response shows, as expected, a characteristic exponential growth (see Fig. 10(d)) [32].

Fig. 11 offers a comparison of the frequency response of a cantilever around the parametric resonance region and above the critical driving voltage. Part a) refers to an isolated cantilever
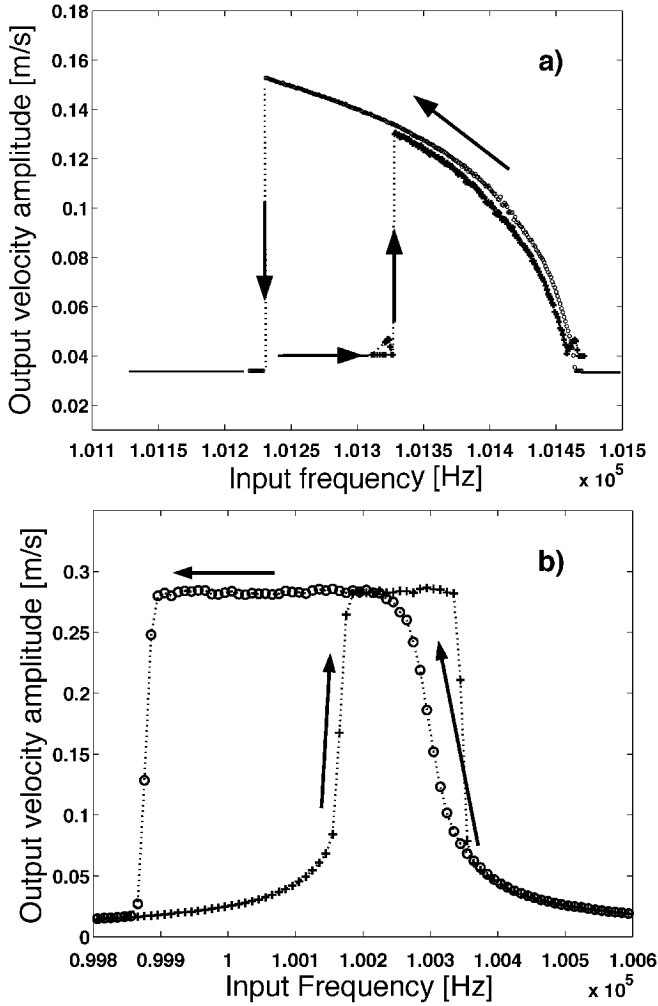
Fig. 11. Frequency response above critical driving voltage: (a) single cantilever and (b) coupled cantilevers in region a) of Fig. 10. Both cantilevers show qualitatively the same behavior, in any one of the three resonant regions.

(data from [19]), part b) to coupled cantilevers and to region a) of Fig. 10. For part b) the data shown corresponds to only one region and only one of the two cantilevers, because qualitatively they show the same behavior, in all three resonant regions. Note also that the flattening of the oscillation amplitude is due to the cantilever touching the substrate. In both cases, uncoupled a) and coupled b), the data was collected by applying a square rooted sinusoidal input and sweeping its frequency from low to high ("+" points) and from high to low ("o" points), as indicated by the arrows.

What we notice is that when sweeping the frequency from low to high, in both cases, the entrance to the parametric region is marked by a sharp jump in the amplitude of the cantilevers oscillation. Since this transition occurs always at the same frequency, related to the natural frequency of the system, the phenomenon has potentially many applications, ranging from mechanical filters to extremely sensitive mass sensors. In the case of two cantilevers, moreover, one has the advantage of having three parametric regions and therefore the option of selecting the frequency range where to work. Note also that the tongues can be placed as desired, at the design stage of the device, by tuning the mechanical coupling coefficient.

Inside the parametric region, as the driving frequency increases, the periodic subharmonic solution is stable and shows decreasing amplitude in case a), and increasing amplitude in case b). We point out again that the flattening of the output is an experimental artifact, due to the fact that the cantilever is touching the substrate. Upon exiting the region, while in case a) the oscillation is reduced to zero, in case b) the periodic solution remains stable and its amplitude virtually keeps increasing, untill it falls back to zero. The location of this second jump is not predictable and depends on the amplitude of the frequency increments. If we invert the process and start decreasing the frequency, the output amplitude starts to increase and keeps increasing, in both cases, even after leaving the parametric region. Again, this large periodic solution eventually collapses to zero at some unpredictable time.

From a dynamical systems point of view, the different behavior in Fig. 11(a) and (b) corresponds to a different phase portrait. In particular, while the single cantilever has a bistable region only on the left side of the tongue, where both the periodic and the trivial solutions are stable, the coupled cantilevers have a bistable region on both sides of the tongue. Interestingly, a single cantilever exhibits a behavior similar to what depicted in Fig. 11(b) when subject to both harmonic and parametric excitation [35], for instance, when excited by a sinusoidal input having a small dc offset. Since the electrostatic force depends on the square of the voltage, this implies that the cantilever is excited both at the driving frequency $\omega$ and at $2\omega$, implying the coexistence of both harmonic ($\omega$) and parametric ($2\omega$) forcing. For the case of two cantilevers this behavior can be explained intuitively by the following approximate argument. From (8) define $x := z_1 + z_2$ and $y := z_1 - z_2$, and consider the case of a square rooted sinusoidal input: the equation of motion are given by

$$\ddot{x} + \left(\bar{\omega}_1^2 + \bar{\epsilon}_1 cos(\omega t)\right) x = -\left(\Delta\omega + \Delta\epsilon cos(\omega t)\right) z_2 \quad (12)$$

$$\ddot{y} + \left(\bar{\omega}_2^2 + \bar{\epsilon}_2 cos(\omega t)\right) y = \left(\Delta\omega + \Delta\epsilon cos(\omega t)\right) z_1 \quad (13)$$

where $\bar{\omega}_1^2 = \omega_1^2 + \gamma_1$, $\bar{\epsilon}_1 = \epsilon_1 + \gamma_2$, $\bar{\omega}_2^2 = \omega_2^2 - \gamma_1$, $\bar{\epsilon}_2 = \epsilon_2 - \gamma_2$, $\Delta\omega = \omega_2^2 - \omega_1^2$, $\Delta\epsilon = \epsilon_2 - \epsilon_1$. Ignoring for the moment their right-hand sides, (12) and (13) represent a pair of uncoupled, standard Mathieu equations. Hence, their parametric regions of the first order are obtained for $\omega = 2\bar{\omega}_1$ and $\omega = 2\bar{\omega}_2$ respectively, which correspond roughly to the peaks of the frequency responses in Fig. 5 and to the values obtained by the previous analysis. From the definition of $x$ we can infer that $z_1$ and $z_2$ oscillate in phase at $\omega = \bar{\omega}_1$, when excited at $\omega = 2\bar{\omega}_1$: hence $z_2$ on the RHS of (12) acts as a harmonic excitation, justifying the phase portrait observed experimentally. A similar argument can be repeated for (13), where $z_1$ oscillates with opposite phase from $z_2$ and provides the harmonic excitation.

## IV. CONCLUSION

In this paper, we have presented a mathematical model for a pair of electrostatically actuated microcantilevers, which explicitly incorporates their dynamical coupling. In our design the cantilevers, which are connected to a common base, constitute the movable plate of microcapacitors and their displacement is independently controlled by the voltage applied across the

plates. In the case of sinusoidal excitation, we have proved that their dynamics are regulated by a pair of *coupled Mathieu* equations. We have provided experimental validation of the mathematical model, including a mapping of the first region of parametric amplification. From this work, many sensing applications can be realized, utilizing the sharp transitions from nonresonant to resonant state, which are present in the parametrically resonant state. Filters and sensors using this mechanism are being explored [11], [12]. In addition, an extension to multi-cantilever arrays is also being investigated. This result offers designers tangible guidelines needed to implement novel parametric devices.

## REFERENCES

[1] M. Despont *et al.*, "VLSI-NEMS chip for parallel AFM data storage," *Sens. Actuators A, Phys.*, vol. A80, no. 2, pp. 100–107, Mar. 10, 2000.

[2] C. Britton *et al.*, "Multiple-input microcantilever sensors," *Ultramicroscopy*, vol. 82, no. 1–4, pp. 17–21, Feb. 2000.

[3] P. Indermhule *et al.*, "Fabrication and characterization of cantilevers with integrated sharp tips and piezoelectric elements for actuation and detection for parallel AFM applications," *Sens. Actuators A, Phys.*, vol. A60, no. 1–3, pp. 186–190, May 1997.

[4] P. Vettiger *et al.*, "The millepeded—nanotechnology entering data storage," *IEEE Trans. Nanotechnol.*, vol. 1, no. 1, pp. 39–55, Mar. 2002.

[5] T. Itoh, T. Ohashi, and T. Suga, "Piezoelectric cantilever array for multiprobe scanning force microscopy," in *Proc. IX Int. Workshop on MEMS*, San Diego, CA, 1996, pp. 451–455.

[6] S. Minne, S. Manalis, and C. Quate, "Parallel atomic force microscopy using cantilevers with integrated piezoresistive sensors and integrated piezoelectric actuators," *Appl. Phys. Lett.*, vol. 67, no. 26, pp. 3918–3920, 1995.

[7] D. Rugar and P. Grutter, "Mechanical parametric amplification and thermomechanical noise squeezing," *Phys. Rev. Lett.*, vol. 67, no. 6, pp. 699–702, Aug. 5, 1991.

[8] T. Kenny, "Nanometer-scale force sensing with mems devices," *IEEE Sensors J.*, vol. 1, no. 2, pp. 148–157, Aug. 2001.

[9] C. Nguyen and R. Howe, "Design and performance of CMOS micromechanical resonator oscillators," in *Proc. IEEE 1994 International Frequency Control Symposium*, 1994, pp. 127–134.

[10] C. Nguyen, "Frequency selective MEMS for miniaturized low-power communication devices," *IEEE Trans. Microwave Theory Tech.*, vol. 47, no. 8, pp. 1486–1503, 1999.

[11] J. Rhodes *et al.*, "Parametrically excited mems-based filters," in *Proc. IUTAM 2003*, Italy, 2003.

[12] R. Baskaran *et al.*, "Experimental characterization of an electrostatically coupled oscillator MEM filter," in *Proc. SEM Annual Meeting, MEMS Symposium*, Milwaukee, WI, 2002.

[13] T. Thundat *et al.*, "Microcantilever sensors," *Microscale Thermophys. Eng.*, vol. 1, pp. 185–199, 1997.

[14] P. Gaucher *et al.*, "Piezoelectric bimorph cantilever for actuation and sensing applications," *J. Phys. IV France*, vol. 8, pp. 235–238, 1998.

[15] B. Chui *et al.*, "Independent detection of vertical and lateral forces with a sidewall-implanted dual-axis piezoresistive cantilever," *Appl. Phys. Lett.*, vol. 72, no. 11, pp. 1388–1390, Mar. 1998.

[16] M. Tortonese, R. Barrett, and C. Quate, "Atomic resolution with an atomic force microscope using piezoresistive detection," *Appl. Phys. Lett.*, vol. 62, no. 8, pp. 834–836, Feb. 1993.

[17] Q. Huang and N. Lee, "A simple approach to characterizing the driving force of polysilicon laterally driven thermal microactuators," *Sens. Actuators A, Phys.*, vol. A80, no. 3, pp. 267–272, March 15, 2000.

[18] M. Napoli and B. Bamieh, "Design of a decoupling controller for electrostatically coupled microcantilevers based on current measurement," in *Proc. 2004 IEEE Amer. Control Conf.*, Boston, MA, 2004.

[19] M. Napoli *et al.*, "A capacitive microcantilever: modeling, validation and estimation using current measurements," *J. Dyn. Sys. Meas. and Control*, June 2004.

[20] R. F. Harrington, *Introduction to Electromagnetic Engineering*. New York: McGraw Hill-Electrical and Electronic Engineering Series, 1958.

[21] MEMSCAP. (2002). [Online]http://www.memscap.com/memrus

[22] K. Turner, P. Hartwell, and N. Macdonald, "Multi-dimensional MEMS motion characterization using laser vibrometry," in *Digest of Technical Papers Transducers'99*, Sendai, Japan, 1999.

[23] *User Manual—Laser Doppler Vibrometer*, 2002.

[24] T. D. Rossing and N. H. Fletcher, *Principles of Vibration and Sound*. New York: Springer, 1999.

[25] M. Yu *et al.*, "Realization of parametric resonances in a nanowire mechanical system with nanomanipulation inside a scanning electron microscope," *Phys. Rev. B—Condensed Matter*, vol. 66, no. 7, pp. 073 406/1–073 406/4, Aug. 15, 2002.

[26] K. Turner *et al.*, "Five parametric resonances in a microelectromechanical system," *Nature*, vol. 396, no. 6707, pp. 149–156, Nov. 12, 1998.

[27] R. Baskaran *et al.*, "Electrostatically coupled MEM oscillators," in *Proc. 2000 ASME Int. Mech. Eng. Cong. Exp.*, 2000.

[28] R. Baskaran *et al.*, "Electrostatic interactions in MEM oscillators," in *Proc. SPIE*, Adelaide, Australia, 2001.

[29] V. Arnold, *Mathematical Methods of Classical Mechanics*: Springer, 1988.

[30] M. Krein, "Foundations of the theory of $\lambda$-zones of stability of a canonical system of linear differential equations with periodic coefficients," *Amer. Math. Soc. Transl.*, vol. 120, no. 2, pp. 1–70, 1983. English translation.

[31] M. Krein and V. Jacubovic, "Hamiltonian systems of linear differential equations with periodic coefficients," *Amer. Math. Soc. Transl.*, vol. 120, no. 2, pp. 139–168, 1983. English translation.

[32] R. Rand. (2001) Lecture Notes on Nonlinear Vibrations. [Online]http://www.tam.cornell.edu/randdocs/

[33] W. Zhang *et al.*, "Effect of cubic nonlinearity on auto-parametrically amplified resonant MEMS mass sensor," *Sens. Actuators A, Phys.*, vol. A102, no. 1–2, pp. 139–150, Dec. 1, 2002.

[34] W. Zhang, R. Baskaran, and K. Turner, "Tuning the dynamic behavior of parametric resonance in a micromechanical oscillator," *Appl. Phys. Lett.*, vol. 82, no. 1, pp. 130–132, Jan. 1, 2003.

[35] M. Napoli *et al.*, "Mathematical modeling, experimental validation and observer design for a capacitively actuated microcantilever," in *Proc. 2003 IEEE Amer. Control Conf.*, Denver, CO, 2003.

**Mariateresa Napoli** received the Ph.D. degree in mechanical engineering from the University of California, Santa Barbara, in 2004. She also received the Ph.D. degree in electrical engineering from the University of Padova, Italy, in 1999.

Currently, she has a postdoctoral appointment with the Department of Mechanical Engineering at the University of California, Santa Barbara. Her research interests include distributed parameters systems, modeling, and control of large arrays of MEMS.

**Wenhua Zhang** (S'03) received the B.S. degree in naval architecture and ocean engineering from ShangHai Jiao Tong University and the M.S. degree in plasma processing from Institute of Mechanics, Chinese Academy of Sciences. He is currently working towards the Ph.D. degree in the Department of Mechanical Engineering at University of California, Santa Barbara.

His research interests are in sensing applications and dynamics of MEMS oscillator.

**Kimberly Turner** (M'02) received the B.S. degree in mechanical engineering from Michigan Technological University in 1994 and the Ph.D. degree in theoretical and applied mechanics from Cornell University, Ithaca, NY, in 1999.

She is currently an Associate Professor of Mechanical and Environmental Engineering at the University of California, Santa Barbara, where she has served on the faculty since 1999. Her research interests include nonlinear dynamics of micro/nanoscale systems, testing and characterization of MEMS devices, modeling of micro/nanoscale devices, and solid-state sensor development.

Dr. Turner is a Member of American Society of Mechanical Engineers (ASME), SEM, AVS, and the Cornell Society of Engineers. She has received the NSF CAREER award, and the Varian Award from the AVS.

**Bassam Bamieh** (S'84–M'91–SM'04) received the electrical engineering and physics degree from Valparaiso University in 1983 and the M.Sc. and Ph.D. degrees from Rice University, Houston, TX, in 1986 and 1992, respectively.

During 1991–1998, he was with the department of Electrical and Computer Engineering and the Coordinated Science Laboratory at the University of Illinois at Urbana-Champaign. He is currently a Professor in the Mechanical Engineering department at the University of California at Santa Barbara, which he joined in 1998. His current research interests are in distributed systems, shear flow turbulence modeling and control, quantum control, microcantilevers modeling and control, and optical actuation via optical tweezers.

Dr. Bamieh is a past receeipient of the AACC Hugo Schuck best paper award, an NSF CAREER award, and is currently an Associate Editor of *Systems and Control Letters*.